Swelling and hydration studies on egg yolk samples via scanning fluid dynamic gauge and gravimetric tests

Pérez-mohedano, R.; Letzelter, N.; Bakalis, S.

DOI:
10.1016/j.jfoodeng.2015.08.014

Document Version
Publisher's PDF, also known as Version of record

Citation for published version (Harvard):
Pérez-mohedano, R, Letzelter, N & Bakalis, S 2016, 'Swelling and hydration studies on egg yolk samples via scanning fluid dynamic gauge and gravimetric tests', *Journal of Food Engineering*, vol. 169, pp. 101-113. https://doi.org/10.1016/j.jfoodeng.2015.08.014

Journal of Food Engineering 169 (2016) 101–113

Contents lists available at ScienceDirect

Journal of Food Engineering

journal homepage: www.elsevier.com/locate/jfoodeng

Swelling and hydration studies on egg yolk samples via scanning fluid dynamic gauge and gravimetric tests

R. Pérez-Mohedano [a, b, *], N. Letzelter [b], S. Bakalis [a]

[a] Centre for Formulation Engineering, Department of Chemical Engineering, University of Birmingham, Edgbaston, Birmingham B15 2TT, UK
[b] Procter & Gamble Innovation Centers Ltd., Whitley Road, Longbenton, Newcastle Upon Tyne, NE12 9TS, UK

ARTICLE INFO

Article history:
Received 11 June 2015
Received in revised form
3 August 2015
Accepted 11 August 2015
Available online 22 August 2015

Keywords:
Scanning fluid dynamic gauge
Gravimetric
Swelling
Food hydration
Fickian diffusion
Moving boundaries

ABSTRACT

Hydration and swelling in initially dry protein-based samples represent the first stage in their cleaning from hard surfaces. These phenomena have been studied in technical egg yolk stains via scanning Fluid Dynamic Gauge (sFDG) and gravimetric tests. Temperature (30 °C to 55 °C) and pH (9.5 to 11.5) were investigated as factors influencing the process. The kinetics did not appear to be significantly different as 95% of the equilibrium swelling was reached at approximately 90 min in all tests. No removal of the egg yolk layer was observed in most cases, except at high alkaline conditions (pH 11.5), where a lift-up followed by a partial removal of the protein network was seen when an external shear stress was applied. The process mimicked creep behaviour of plastic materials. Gravimetric data on the hydration of the sample suggested a Fickian diffusion transport (Case I), where solvent diffusion is the rate limiting stage. The initial hydration was proved to be linear. Two diffusion theories of increasing complexity were applied to estimate effective diffusion coefficients: Fick's second law (with moving boundaries) and a non-linear poroelasticity theory. The temperature dependence of different diffusion coefficients assuming an Arrhenius equation gave an activation energy in the range of 16.4 (±6.7) KJ/mol to 18.4 (±9.0) KJ/mol.

1. Introduction

Foods are complex examples of soft condensed matter (Mezzenga et al., 2005; van der Sman and van der Goot, 2009; Van Der Sman, 2012). Their physical and chemical properties show a strong dependence on moisture content (Labuza and Hyman, 1998). If low hydrated food samples are exposed to high moisture or liquid environments, the absorption of water into the food matrix can occur. This process leads, in certain occasions, to a change in the volume of the sample (swelling) and takes place until thermodynamic equilibrium is reached.

The reader must differentiate between *degree* of swelling and *kinetic* of swelling when a hydration phenomenon with an associated change in thickness occurs. *Degree* of swelling indicates the net increase in volume occurring in the sample over time. A swelling-ratio coefficient, typically defined as the ratio between the volume at equilibrium and the volume at dry state of the sample, is used to characterise this process. *Kinetic* of swelling relates to the speed at which the equilibrium is reached. It is typically characterised by a diffusion coefficient (Ganji, 2010).

Numerous approaches have been followed to model swelling/hydration phenomena in different foods. Some aim to fit experimental data by using empirical models. For example, this was done by Chen et al. (2007) for the modelling of swelling on cross-linked corn starch granules; by Davey et al. (2002) for the hydration of rice grains of different sizes and at different temperatures; by Kruif et al. (2015) on the swelling study of casein hydrogels; or by Malumba et al. (2013) on the behaviour of wheat starch granules subjected to different thermal treatments. Also, the estimation of intrinsic parameters is of interest. Bakalis et al. (2009), Bello et al. (2010) or Oztop and McCarthy (2011) estimated diffusion coefficients on rice, cereals and protein-based gels respectively. Increasing the complexity of the analysis leads to develop theoretical models on the mass transport and swelling behaviour of different foodstuff as done by Briffaz et al. (2014) or Chapwanya and Misra (2015). The most complex models developed required the use of advanced computational systems to numerically solve the equations given.

* Corresponding author. Centre for Formulation Engineering, Department of Chemical Engineering, University of Birmingham, Edgbaston, Birmingham B15 2TT, UK.
E-mail address: PMR005@bham.ac.uk (R. Pérez-Mohedano).

http://dx.doi.org/10.1016/j.jfoodeng.2015.08.014

Nomenclature

A	cross sectional area
C	mass concentration expressed as dry basis moisture content (water mass uptake/dry solid sample mass)
C_0	initial moisture content (water mass at time 't = 0'/dry solid mass sample)
C_∞	moisture content at equilibrium 't = ∞'
D	effective diffusion coefficient
D_0	maximum effective diffusion coefficient
D_F	effective diffusion coefficient for Fick's equation
D_{NL}	effective diffusion coefficient for non-linear poroelasticity theory
E_A	activation energy
h_0	initial thickness. Thickness at time 't = 0'
h_{dry}	sample thickness at dry state
$h(t)$	thickness at time 't'
$\overline{h(t)}$	normalised thickness at time 't'
h_∞	thickness at equilibrium
k, k′	constants incorporating characteristics of macromolecule and penetrant system
M_0	initial sample mass. Sample mass at time 't = 0'
M_{dry}	dry sample mass
$M(t)$	total sample mass at time 't'
$\overline{M(t)}$	normalised sample mass at time 't'
M_∞	total sample mass at equilibrium (t = ∞)
n, n′	diffusional exponents
N	effective number of polymer chains per unit volume of the polymer (n° chains/m^3 polymer)
R	gas constant
t	time
T	temperature
x,y,z	Cartersian coordinates
Z	field of markers

Greek symbols

Ω	volume per solvent molecule (m^3/solvent molecule)
λ	stretch in uniaxial direction (thickness at time 't'/dry state thickness)
λ_0	initial stretch in uniaxial direction (initial thickness/dry state thickness)
ρ_f	density of the wash solution
χ	Flory–Huggins parameter (interaction between the solvent and the polymer)

Abbreviations

sFDG	scanning fluid dynamic gauge
HDL	high-density lipoproteins
LDL	low-density lipoproteins

Examples of this latter case can be found in Mitchell and O'Brien (2012) or Van Der Sman (2014).

Swelling is essential in the cleaning of initially dried protein soils in alkali conditions (Fryer et al., 2006). The phenomena involves three stages (Bird and Fryer, 1991). Initially, the sample swells as the wash solution diffuses into the soil network. Once the sample reaches a certain degree of hydration, an erosion process occurs as a consequence of the application of an external mechanical action (shear stress) and/or the hydrolysis reactions due to the presence of chemicals such as enzymes or high alkalinity. When the removal is nearly finished, the importance of the adhesion forces arises and the process slows down until complete cleaning is achieved.

Extensive research has been already performed to study swelling and dissolution phenomena in simple protein-based systems (β-lactoglobulin). A *dissolution threshold* was reported as a function of pH and the volume fraction available in the protein network. Below this threshold, swelling-ratio increased with the increase of alkalinity (Mercadé-Prieto et al., 2007a). Dissolution was possible at certain alkalinity (above pH threshold) and above a certain swelling-ratio (volume-fraction threshold) (Mercadé-Prieto et al., 2009, 2007b, 2007c). Non-covalent intermolecular bonds were hydrolysed due to alkali denaturation and disengaged molecules were transported to the bulk solution. Dissolution rates were found to vary as a function of alkalinity, ionic strength and protein structure (Mercadé-Prieto and Chen, 2006). These studies were expanded by Saikhwan et al. (2010) where different swelling behaviours were observed for different protein systems.

With the introduction of novel techniques to measure swelling, such as the scanning fluid dynamic gauge –sFDG– (Gordon et al., 2010), new possibilities arise to study different soils, substrates or testing conditions (temperature, chemistry and mechanical forces). Swelling phenomenon and its link to cleaning is yet a field that can be further explored. The purpose of this study is to describe swelling and hydration in egg yolk (protein-based) samples. Egg yolk deposits are highly difficult to remove from a hard surface when dried and are one of the typical consumer complaints within the automatic dishwasher industry (DuPont, 2012). Modelling of swelling is a key step in order to fully describe the removal of the egg soil. With this aim, swelling and water uptake in dried egg yolk samples have been studied as a function of temperature and pH. Scanning Fluid Dynamic Gauge (thickness measurements) and gravimetric data have been analysed and compared. Different diffusional theories have been used to describe the type of mass transport occurring and to evaluate the accuracy to predict swelling in detail. These theories are presented in the section below.

2. Diffusional theories

Alfrey et al. (1966) proposed a classification on the diffusional transport occurring based on the rate limiting stage. According to this classification, *Fickian diffusion or Case I* occurs when the solvent diffusion rate is clearly slower than the network relaxation rate. Relaxation time describes the time required for the sample network to accommodate to the increase in liquid content. It is related to the transition from glass to rubber state of the sample. A *Non-Fickian* transport process or *Case II* takes place when liquid mobility is much higher than the structure relaxation time (Thomas and Windle, 1982, 1980). In between these two extreme cases, an *anomalous transport* can also be defined. Liquid movement and relaxation time are in the same order of magnitude.

2.1. Power-law model

Peppas & J.L.Sinclair (1983) presented a semi-empirical equation (Eq. (1)) to assess the type of transport occurring in one-dimensional (thin slabs) isothermal processes. The equation is valid for the first 60% of the mass uptake $\left(\frac{M(t)}{M_\infty} < 60\%\right)$ under perfect sink conditions (i.e. infinite supply of solvent).

$$\frac{M(t)}{M_\infty} = kt^n \quad (1)$$

where:

- $M(t)$: Total sample mass at time 't'. [=] kg.
- M_∞: Total sample mass at equilibrium (t = ∞). [=] kg.
- k: Constant incorporating the characteristics of the macromolecule and the penetrant system.
- t: Time. [=] s.
- n: Diffusional exponent.

Depending on the value of the diffusional exponent 'n', any transport mechanism can be identified. Table 1 illustrates the different cases.

Different geometries (other than the slab) or in particular, the increase of thickness of the sample when hydrating, can lead to a variation in the estimated values of 'n' (Peppas and Brannon-Peppas, 1994). The increase of thickness over time implies longer distances for a solvent molecule to travel but also higher holding capacity of the sample, as the volume achieved at equilibrium is higher. The presence of a higher number of solvent molecules implies an extra resistance for the network to adapt to the changes. In consequence, its relaxation time increases with the increase of swelling-ratio. Other factors affecting the diffusional exponent 'n' are the use of monodisperse or polydisperse solvent systems. In the presence of a particle size distribution in the solvent, small molecules are able to diffuse faster through the sample network at early stages, but the equilibrium might be delayed as larger molecules move slower in the final stages. A change in the assumption of boundary perfect sink conditions can lead to variations in the diffusional exponent 'n' as well. This assumes an instantaneous equilibrium between the solvent and the top layer of the sample once they come into contact. However, even though the equilibrium might be reached fast, it cannot be instant.

Eq. (1) was adapted in this work to fit the sFDG data by replacing mass by height. The analogue expression is shown in Eq. (2).

$$\frac{h(t)}{h_\infty} = k' t^{n'} \quad (2)$$

where:

- $h(t)$: Thickness at time 't'. [=] m.
- h_∞: Thickness at equilibrium (t = ∞). [=] m.
- k′: Constant (for sFDG data).
- t: Time. [=] s.
- n′: Diffusional exponent (for sFDG data).

2.2. Fick's second law

If Fickian diffusion is the predominant type of transport, Fick's second law (Eq. (3)) can be used to fit experimental data (Bird et al., 2007). Eq. (3) describes the uniaxial concentration change over time occurring for a thin slab geometry.

$$\frac{\partial C}{\partial t} = D_F \frac{\partial^2 C}{\partial z^2} \quad (3)$$

where:

- $C = \frac{M(t)}{M_{dry}}$: Mass concentration (expressed relative to the initial dry weight of the soil). [=] kg. Water content/kg. Dry sample mass.
- $M(t)$: Total sample mass at time 't'. [=] kg.
- M_{dry}: Dry sample mass. [=] kg.
- t: Time. [=] s.
- D_F: Effective diffusion coefficient for Fick's equation. [=] m^2/s.
- z: Uniaxial diffusion direction. [=] m.

A series of assumptions are typically made when this equation is used (Sam Saguy et al., 2005). The most common ones involve:

- No other transport mechanisms are considered (e.g. capillarity).
- The effective diffusion coefficient is constant and independent of the moisture content in the network.
- Only the diffusion of unreacted liquid is modelled.
- The initial moisture content in the network is uniform (i.e. isotropic state).
- No resistances to the flux are found at the top layer and therefore the equilibrium occurs instantly.
- Swelling or shrinkage phenomena are typically not considered.
- The geometry is simplified to slab, spheres or cylindrical shapes.
- Heat transfer equations are commonly ignored.

In a diffusion process with a change in volume (thickness) of the sample, boundary conditions are constantly varying. If the degree of swelling reaches a significant level (e.g. doubles up), and this is not considered by the model, wrong conclusions can be made when analysing the results. The assumption of molecular incompressibility (additive volumes) can relate the thickness change with the mass gained for a uniaxial swelling case via a density relationship. This is expressed in Eq. (4).

$$M_f = M(t) - M_0 = \rho_f \cdot A \cdot (h(t) - h_0) \quad (4)$$

where:

- $M(t)$: Total sample mass at time 't'. [=] kg.
- M_0: Initial sample mass. Sample mass at time 't = 0'. [=] kg.
- ρ_f: Density of the wash solution. [=] kg/m^3.
- A: Cross sectional area. [=] m^2.
- $h(t)$: Thickness at time 't'. [=] m.
- h_0: Initial thickness. Thickness at time 't = 0'. [=] m.

The incorporation of Eq. (4) into Eq. (3) allows the calculation of diffusion profiles considering moving boundaries.

2.3. Non-linear poroelasticity theory

Classical Biot's theory of poroelasticity (Biot, 1941), adapted from Gibbs (1906), in combination with statistical mechanics (Flory and Rehner Jr., 1943) has been used extensively to analyse solvent migration in polymer systems. Hong et al. (2008) developed a non-linear approach that combines a non-equilibrium thermodynamic theory with a Fickian kinetic law to analyse the diffusion of small molecules into a neutral polymer gel. Mass transport was analysed together with the deformation of the polymer. The theory expands

Table 1
Types of mass transport as a function of the diffusional exponent 'n'. Coefficients are valid for one-dimensional (slab) isothermal processes.

Type of transport	Diffusional exponent (n)	Time dependence
Fickian Diffusion (Case I)	0.5	$t^{1/2}$
Anomalous transport	0.5 < n < 1	t^{n-1}
Non-Fickian transport (Case II)	1	Time independent

Fick's second law by introducing intrinsic properties of the solvent and polymer.

- N: Effective number of polymer chains per unit volume of the polymer. It is defined as a constant value and refers to a reference condition at dry state. [=] n° chains/m^3 polymer.
- Ω: Volume per solvent molecule [=] m^3/solvent molecule.
- χ: Flory–Huggins parameter (interaction between the solvent and the polymer).

The kinetics of the solvent molecules is considered to follow a Fickian diffusion model. It is characterised by a diffusion coefficient, D_{NL}, which is isotropic and independent of the concentration and deformation gradients. By considering a uniaxial swelling (constraint in 2 directions) and an isotropical initial swollen state, the stretch of the network as a function of time and position is given by Eq. (5).

$$\lambda_0^2 \frac{\partial \lambda}{\partial t} = D_{NL} \frac{\partial}{\partial Z}\left(\xi(\lambda)\frac{\partial \lambda}{\partial Z}\right) \tag{5}$$

where:

$$\xi(\lambda) = \frac{1}{\lambda_0^2 \lambda^4} - \frac{2\chi\left(\lambda_0^2\lambda - 1\right)}{\lambda_0^4 \lambda^5} + N\Omega \frac{\left(\lambda_0^2\lambda - 1\right)\left(\lambda^2 + 1\right)}{\lambda_0^2 \lambda^4} \tag{6}$$

where:

- λ_0: Initial stretch in uniaxial direction (initial thickness/dry state thickness).
- λ: Stretch in uniaxial direction (thickness at time 't'/dry state thickness).
- D_{NL}: Effective diffusion coefficient for Non-Linear theory. [=] m^2/s.
- t: Time [=] s.
- Z: field of markers along z-axis (define network stretch reference points).

The total thickness of the sample can be calculated as:

$$h(t) = \int_0^{h_{dry}} \lambda(z,t)dz \tag{7}$$

where:

- $h(t)$: Thickness at time 't'. [=] m.
- h_{dry}: Layer thickness in the dry state. [=] m.
- λ: Stretch in uniaxial direction (thickness at time 't'/dry state thickness).
- z: Uniaxial diffusion direction. [=] m.

Also, an algebraic equation (Eq. (8)) relates the equilibrium swelling ratio, λ_∞, with λ_0, N, Ω and χ as follows:

$$ln\left(\frac{\lambda_0^2\lambda_\infty - 1}{\lambda_0^2\lambda_\infty}\right) + \frac{1}{\lambda_0^2\lambda_\infty} + \frac{\chi}{\lambda_0^2(\lambda_\infty)^2} + \frac{N\Omega}{\lambda_0^2}\left(\lambda_\infty - \frac{1}{\lambda_\infty}\right) = 0 \tag{8}$$

2.4. Temperature dependence

For the case of the diffusion of a fluid into a solid, the effective diffusion coefficient at different temperatures typically follows an Arrhenius equation (Mehrer, 2007) (Eq. 9).

$$D = D_0 \cdot e^{-E_A/RT} \tag{9}$$

where:

- D: Effective diffusion coefficient. [=] m^2/s.
- D_0: Maximum effective diffusion coefficient. [=] m^2/s.
- E_A: Activation energy. [=] J/mol
- R: Gas constant [=] J/mol K.
- T: Temperature. [=] K.

3. Materials & methods

3.1. Egg yolk samples

Egg yolk was chosen as the food material studied. It is a complex mixture of proteins and lipids. Its typical dry composition comprises 33% of proteins, 62.5% of fats, less than 3.5% of minerals and 1% of carbohydrates approximately (Mine and Zhang, 2013). Two phases can be separated: plasma and granules. Despite the larger proportion of fats, samples are considered protein-based as their physico-chemical properties depend on the protein network that forms the main structure. Egg yolk is formed by high (HDL) and low-density lipoproteins (LDL) consisting on spherical particles that surround a lipid core. LDLs are the essential components that allow the emulsification of egg yolk due to their amphiphilic properties. Also, preheated samples above 70 °C have been reported to form a gel system due to the aggregation of protein networks occurring at high temperatures (Denmat et al., 1999; Tsutsui, 1988). At alkaline conditions, the network hydrates and swells.

Samples were obtained from Centre for Testmaterials (product DS-22, C.F.T. BV, Vlaardingen, the Netherlands). The samples, widely used for detergent tests, were made of a sprayed layer of egg yolk over a stainless steel base. Size of the tiles was 12 cm × 10 cm with 1.75 g (±0.04 g) of egg yolk deposited on and an estimated initial thickness of 68 μm (±14 μm). The initial thickness was calculated by extrapolating the data collected from sFDG experiments, which led to a relatively high standard deviation.

The initial moisture content was obtained by weighing 3 samples before and after they were deposited in a vacuum oven at 60 °C during 8 h (Booth, 2003). 0.11 g (±0.03 g) were lost as an average during this process. Therefore, the initial moisture content (C_0) was estimated as 0.067 g water/g. dry sample. The amount of water initially present in the samples corresponds to a layer thickness of 9 μm. This value was estimated as the thickness of a water layer of 0.11 g homogeneously distributed across the area of the tile.

3.2. Scanning fluid dynamic gauge

Fig. 1 shows a schematic of the scanning fluid dynamic gauge (sFDG).

The technique allows the real time measurement of the thickness of immobile soft soil samples submerged in a liquid environment (Gordon et al., 2012). Samples are placed in the upper tank and thickness is measured thanks to a proximity nozzle through which a gravity-maintained flow is created. The variation in the soil thickness (swelling or removal) over time is a consequence of its contact with the liquid solution and the surface shear stress generated by the gauging flow through the nozzle. The scanning

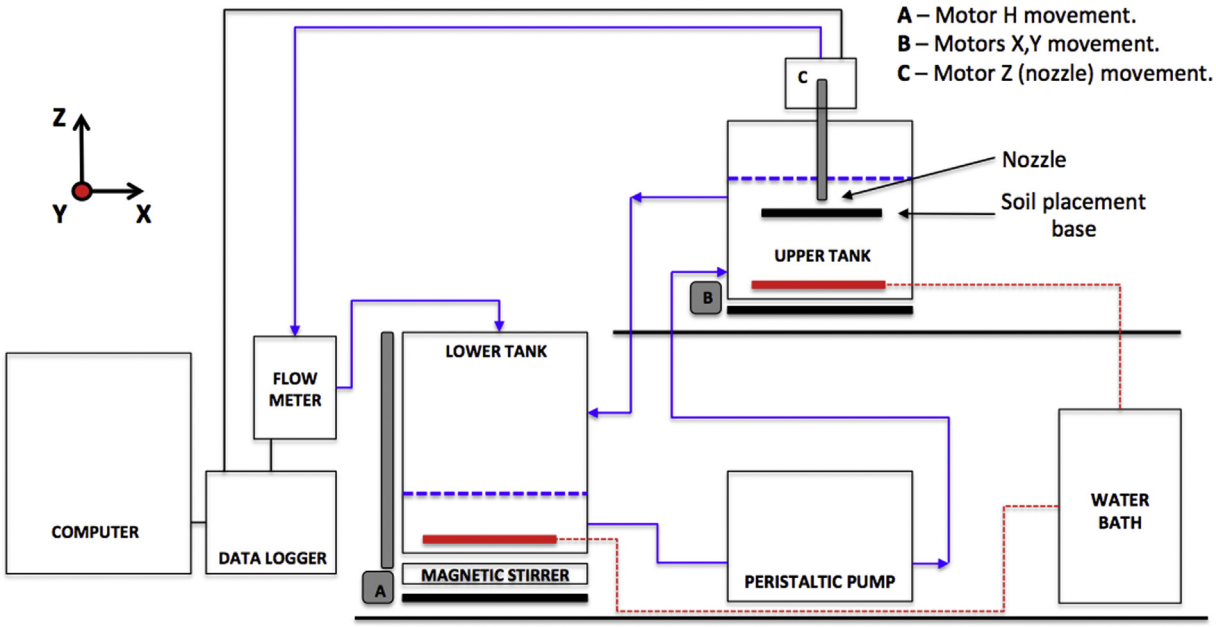

Fig. 1. Schematic of the scanning fluid dynamic gauge.

mode enables the analysis of multiple locations. The following parameters can be studied: soil type, temperature, chemistry level (pH, enzymes, ionic strength), net shear stress applied over the sample and frequency of application of shear stress per location. The frequency factor is defined as the ratio of time the gauging fluid is imposing a surface shear stress on a particular location over the total experimental time. For more detailed information the reader is referred to Tuladhar et al. (2000, 2002); Gordon et al. (2010).

sFDG raw data consist of thickness values at different times per location. For a particular location, the frequency at which shear stress is applied determines the separation between groups of data points. In order to compare thickness values from different locations, a polynomial fitting was performed for each individual location. The degree of the polynomial was set at the lowest possible (6th degree or lower) to produce an acceptable fit ($R^2 > 0.98$). Thickness values were then calculated at fixed times (i.e. every minute) and compared against the other locations and triplicates. An average trend line with its associate error was finally estimated for each experimental condition considered.

3.3. Design of experiments and experimental procedure

Temperature and pH were selected as the factors to study for both sFDG and gravimetric tests. Preliminary studies showed that the effect of pH on swelling was higher than temperature. Therefore, for the design of experiments 3 levels were selected for pH (9.5, 10.5 and 11.5) and 2 levels for temperature (30 °C and 55 °C), in agreement to the values typically found in commercial automatic dishwashing. This resulted in a combination of 6 different set-ups as shown in Table 2. Triplicates were measured for each case and the order of the experiments randomized. Tests were run for 180 min.

Table 2
Design of experiments.

Experiment	Temperature	pH
1	30 °C	9.5
2	55 °C	9.5
3	30 °C	10.5
4	55 °C	10.5
5	30 °C	11.5
6	55 °C	11.5

Deionised water was used and the hardness set at 8.5 US gpg (4.4 mM) with 0.236 g/l $CaCl_2 \cdot 6H_20$ and 0.076 g/l $MgCl_2 \cdot 6H_20$ (molar ratio between $CaCl_2 \cdot 6H_20$ and $MgCl_2 \cdot 6H_20$ was 3:1). To provide the necessary pH, buffer solutions were prepared and pH measured with a pH meter (product Orion 4 Star™, Thermo Scientific Orion).

- For pH 9.5, 0.112 g/l of Na_2CO_3 and 0.150 g/l of $NaHCO_3$ were used ($[Na_2CO_3] = 1.10$ mM and $[NaHCO_3] = 1.80$ mM).
- For pH 10.5, 0.106 g/l of Na_2CO_3 were added ($[Na_2CO_3] = 1.00$ mM).
- For pH 11.5, 0.13 g/l of NaOH were added ($[NaOH] = 3.25$ mM).

Before running the experiments, all chemicals were added to the lower tank and stirred and recirculated through the system for 10 min. Temperatures in both tanks were monitored constantly with the aid of waterproof digital thermometers.

For the sFDG runs, 4 points were analysed per sample to asses the variability within a tile. The position of the nozzle changed every minute and shear stress over a particular location was applied for approximately 30 s in intervals of 4 min. Therefore, the frequency factor was set about 12–13% of the total experimental time. Shear stress applied over the samples was kept constant at 18 Pa. Underneath the nozzle a pressure change and a tensile force are generated as a consequence of the fluid moving upwards through the nozzle. The pressure change and pull-force were estimated by applying Bernoulli's equation (Gordon, 2012). With the set-up considered these values were established at 500 Pa and 1.6 mN approximately. Fig. 2 illustrates the locations studied over the samples.

Gravimetric tests were conducted in the upper tank of the sFDG apparatus. Samples were placed on the soil platform without any gauging action occurring. They were taken out at specific times for their weight measurement: 3, 6, 10, 15, 20, 25, 30, 40, 50, 60, 80, 100, 120, 150 and 180 min. Prior to the measurement, the base was

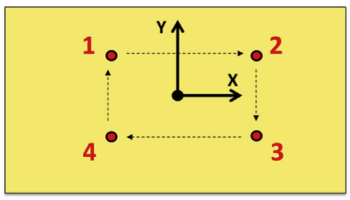

POINT	X (mm)	Y (mm)
1	-20	20
2	20	20
3	20	-20
4	-20	-20

Fig. 2. Schematic of points analysed while using sFDG.

dried and the excess surface water was removed by soft-shaking the tiles 10 times. They were weighed on a digital scale (product EP201, Ohaus) with a readability of ±0.01 g. Once an experiment was completed, the tile was cleaned, dried and weighed again so the net sample mass could be estimated.

3.4. Comparison of sFDG and gravimetric data

The *kinetics* (time to equilibrium) of both sFDG and gravimetric data were initially studied using a dimensionless approach. Data were normalised by applying Eq. (10) and Eq. (11):

$$\text{For sFDG data}: \quad \overline{h(t)} = \frac{h(t) - h_0}{h_\infty - h_0} \tag{10}$$

$$\text{For Gravimetric data}: \quad \overline{M(t)} = \frac{M(t) - M_0}{M_\infty - M_0} \tag{11}$$

where:

- $\overline{h(t)}$ = Normalised thickness at time 't'.
- $\overline{M(t)}$ = Normalised sample mass at time 't'.

The relative values (0–1 scale) indicated the equilibrium degree achieved at any experimental time. This approach made all experiments comparable independently of the degree of swelling or hydration. The comparison was also done in absolute values by transforming thickness data into mass data using Eq. (4).

3.5. Solution of equations from diffusional theories

Equations from Fick's second law (Eq. (3) and Eq. (4)) were solved via an algorithm developed in MATLAB® using a forward finite difference method. It was assumed that the bottom of the sample ($z = 0$) was attached to a rigid surface with no diffusion occurring at this position. Also, the top face ($z = h(t)$) was considered to be freely exposed to the solvent. Thus, liquid penetration occurred from top to bottom. The sample was considered to swell uniformly in one direction (z), with a constrained or negligible lateral stretch. At each time step, swelling of the sample (Eq. (4)) was incorporated and the total thickness was discretised again to compute for this change. The assumption of an instantaneous equilibrium at the boundary layer between the network and the fluid together with a zero flux at the bottom layer were considered as boundary conditions. Additionally, the diffusional coefficient was assumed to be constant and independent of the moisture gradient. The initial condition assumed a homogeneous distribution of the initial moisture content within the sample. The boundary and initial conditions are expressed as follows:

- Initial Condition: $t = 0 \rightarrow C = C_0$
- Boundary Condition 1: $C(z = h(t)) = C_\infty$
- Boundary Condition 2: $z = 0 \rightarrow \frac{\partial C}{\partial z} = 0$

The effective diffusion coefficient values (D_F) were calculated by minimising the error between experimental and numerical results.

The same assumptions used for Fick's second law were considered to solve the equations from non-linear theory (Eq. (5) and Eq. (8)). A forward finite difference method was used to determine a solution for Eq. (5). The initial condition assumed an isotropical swollen state with an initial swelling ratio of λ_0. Boundary conditions established the instantaneous equilibrium at the top surface (BC1: $\lambda\,(z = h(t)) = \lambda_\infty$) and the condition of zero flux at the bottom surface (BC2: $\frac{\partial \lambda}{\partial z}(z = 0) = 0$). After a long time ($t \rightarrow \infty$) the system evolved to an equilibrium state ($\lambda = \lambda_\infty$). Stretch profiles obtained (λ) were integrated over the layer thickness in the dry state (h_{dry}) by applying Eq. (7) to calculate net thickness values over time. Eq. (8) was used to relate the equilibrium stretch (λ_∞) with λ_0 and other intrinsic parameters: N, Ω and χ.

The initial swelling ratio (λ_0) and the equilibrium stretch (λ_∞) needed for the calculations were obtained from experimental data.λ_0 was estimated by dividing the initial experimental thickness ($h_0 = 68\ \mu m$) over the dry thickness ($h_{dry} = 68\ \mu m – 9\ \mu m$), giving $\lambda_0(t = 0) = 1.1$. The different λ_∞ were estimated for each case by dividing the thickness at equilibrium over the dry thickness (h_{dry}). The volume of a solvent (water) molecule (Ω) was $3 \cdot 10^{-29}$ m^3/molecule. As three variables were unknown (χ, N and D_{NL}) and there were two available equations (Eq. (5) and Eq. (8)) an iterative process was established.

Finally, D_0 an E_A values were estimated for data points at the same pH and different temperatures by using Eq. (9). Despite the lack of rheological information, the soil sample was assumed to behave as a solid as it did not flow in any experimental condition and it was partly detached from its surface when a sufficiently high external force was applied. This analysis was carried out with the intention of evaluating the suitability of the techniques used in the estimation of D_0 and E_A. The use of only two temperatures in the study did not allow any deeper insight to be made.

4. Results & discussion

4.1. sFDG and gravimetric results

Data collected experimentally was processed according to the methodology explained in the previous section. Thickness and mass values were initially represented over time. Fig. 3 shows the results for gravimetric (A) and sFDG experiments (B & C).

The plots show the rapid increase of thickness or mass that occurred during the initial minutes of any experimental run (i.e. 40 min). The rate decreased over time as the samples approached the equilibrium. The end point was different depending on the experimental conditions. Data demonstrated that by increasing temperature and pH, swelling and water uptake increased. The effect of pH on the hydration process was more important than

temperature within the levels studied. This is clearly seen in Fig. 3A for gravimetric tests. Equilibrium was reached by the end of the experimental time for all the conditions studied. The system was considered equilibrated when the swelling or mass-uptake rate was less than 5% of the swelling rate in the first 3 min of the experiment.

For sFDG measurements, the variability between the 4 locations analysed within a sample was found to be about 4% of the measured thickness. The variability increased up to about 10% when different samples were compared. This indicated higher differences between samples than at different locations on a single tile. For gravimetric tests, the variability was lower at around 3% of the measured weight. The higher error seen for sFDG measurements was due to an accumulation of errors from different factors such as the application of a shear stress over the sample, the error related to the movement of the nozzle around different positions, the inner error of the flowmeter, the accuracy of the z-motor and the possible inhomogeneity of the sample at the different locations considered.

At 55 °C and pH 11.5, localised blisters appeared on the surface after 2 h as shown in Fig. 4. We believe that these blisters related to hydrolysis reactions occurring at high alkalinity. Peptide bonds broke (cohesive failure) as a consequence of the high concentration of OH^- ions and the network strength weakened (Saikhwan et al., 2010). A distortion of the data was thus observed as the presence of big blisters allowed the solvent to penetrate more easily into the network. This would explain the higher weight and variability seen after 150 min for the gravimetric tests (Fig. 3A). This weakness in the soil called for extra care when handling the tiles in order to prevent the loss of any soil when measuring their weight.

Similar issues were found for sFDG tests at the same experimental conditions. A lift-up effect or removal of the soil was observed in some of the locations studied. The lift-up effect consists of the stretch of the network due to the pull force produced by the liquid suction through the nozzle of the sFDG. The measured thickness increases in consequence. The removal of the sample occurs when the action of the sFDG over the soil surface is high enough to detach some of the top layers. The consequence is that a lower thickness is measured. Fig. 5 shows the raw data collected for the three experiments done at 55 °C and pH 11.5 for each of the 4 locations analysed. The graphs illustrate the different behaviours commented. Overall, among the 12 different locations studied, a lift-up effect was observed 5 times followed by a removal of the soil in 3 occasions. These cases were disregarded when estimating the average thickness profile for that sample. For the locations showing an apparent equilibrium we assumed none of these effects occurred.

Fig. 6 summarises the possible scenarios observed for the measurement of thickness using the sFDG.

The difference in thickness between lift-up and equilibrium cases within a single replicate represents the stretch occurring in a specific location. Fig. 7 represents that difference for the location 3 in the test shown in Fig. 5A. The curve mimics creep profiles observed in plastic or polymeric materials (McKeen, 2015). Creep is defined as the change over time that occurs to a material when subjected to a constant or regular stress. Those locations with a lift-up effect deformed plastically, not elastically, as they did not return to the original shape every time the tensile force was applied. Creep

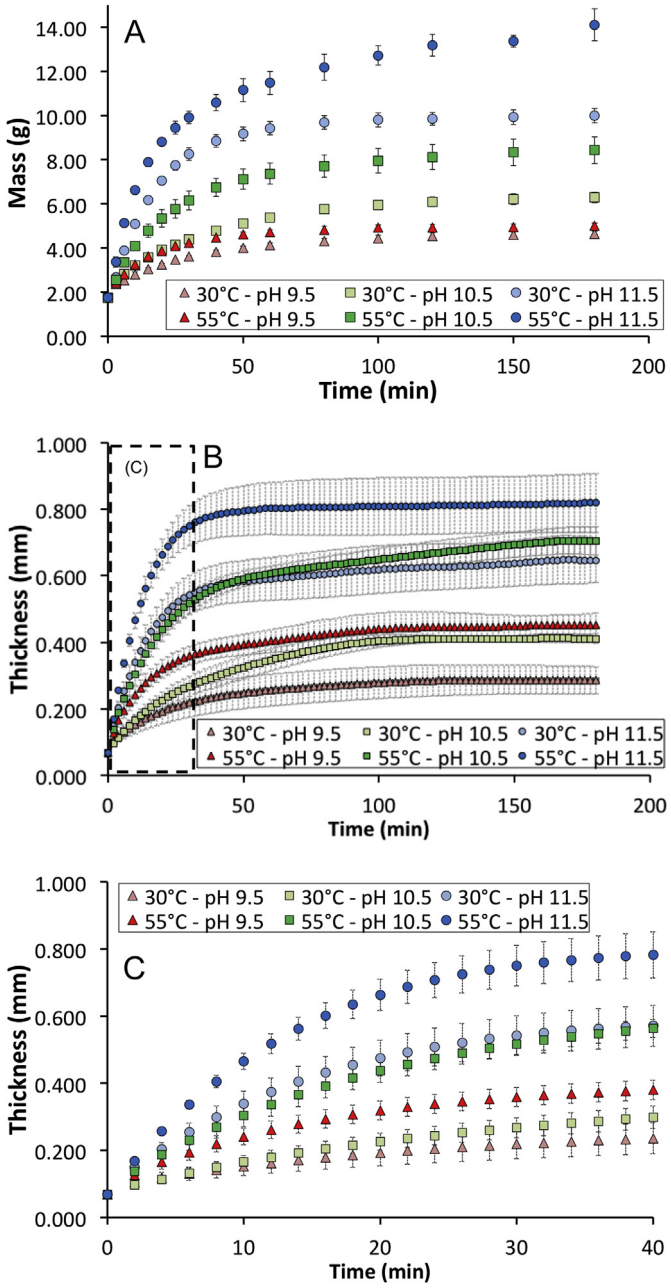

Fig. 3. Experimental results. A – Gravimetric tests. B – Polynomial fit and averaged sFDG data. C – sFDG data for the first 40 min.

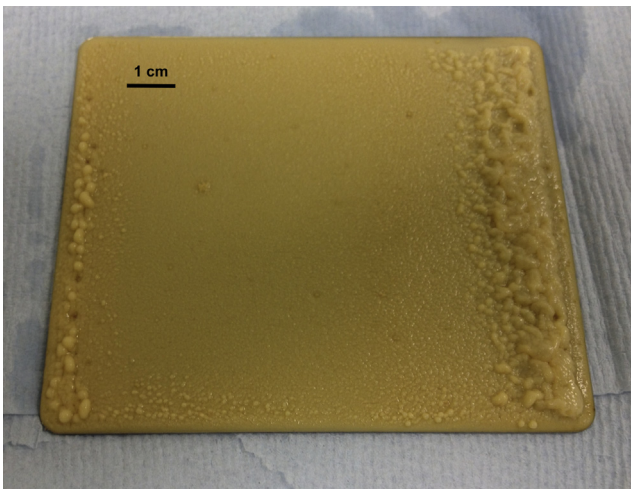

Fig. 4. Egg yolk tile showing blisters at the edges after being submerged in a solution at 55 °C and pH 11.5 for 180 min.

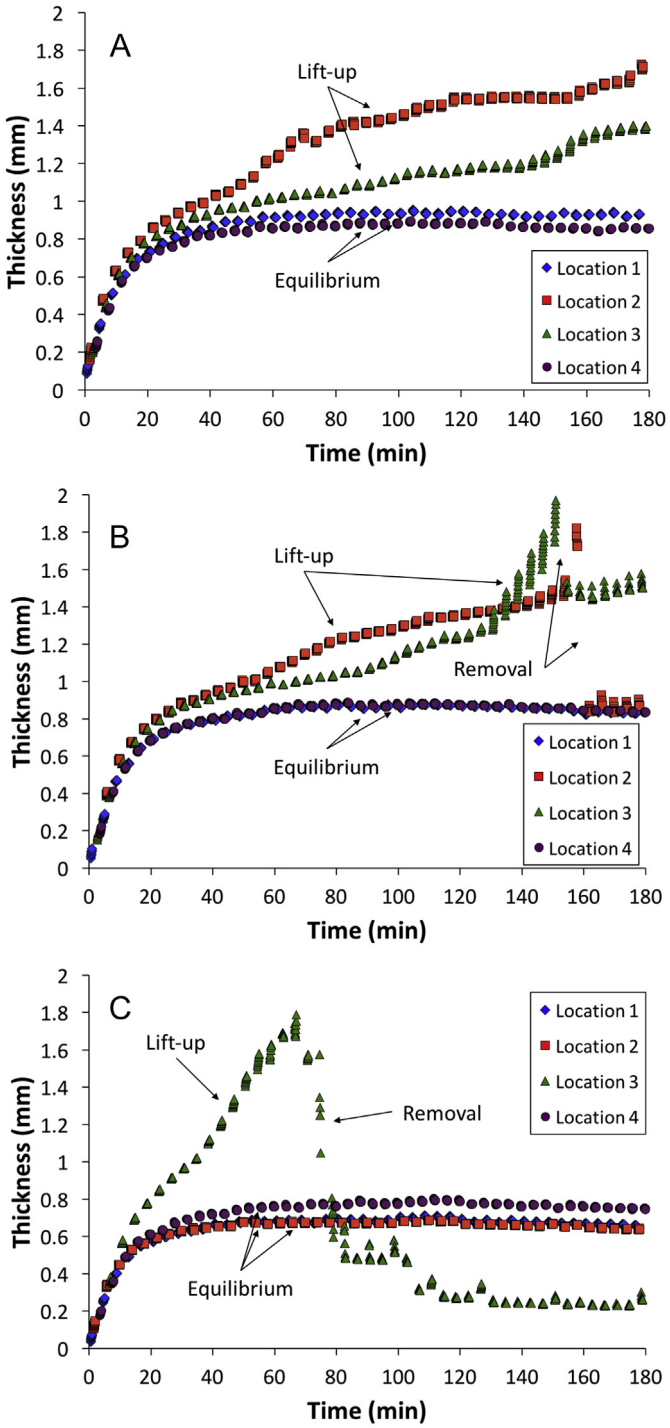

Fig. 5. sFDG raw experimental data at 55 °C and pH 11.5. A – First test; B – Second test; C – Third test; Blue diamonds, red squares, green triangles and purple circles represent locations from 1 to 4 respectively. (For interpretation of the references to colour in this figure legend, the reader is referred to the web version of this article.)

curves typically show three stages: primary, secondary and tertiary. The primary stage is an initial and non-steady deformation on the sample. This is followed by a constant strain rate, which characterises the secondary stage. Finally, when the stretch is high enough, the material starts to fail and the strain accelerates. This last stage precedes the fracture point, where the sample finally breaks. This phenomenon could be identified at a different extent in each of the cases not following an equilibrium trend. These observations arise the suitability of the sFDG in the analysis of creep behaviour of different materials and at different conditions (i.e. temperature, degree of swelling or tensile force applied).

4.2. Comparison of sFDG and gravimetric data

In Fig. 8 normalised gravimetric, $\overline{M(t)}$ (x-axis), and sFDG, $\overline{h(t)}$ (y-axis), data are shown. Results compare the kinetics of the process. They were separated for every pH level considered. The colour scale indicates the time the measurements were undertaken. Samples started at the beginning of the axis and dimensionless height and mass increased with time as samples reached equilibrium.

Good agreement between the techniques was observed at pH 9.5 (Fig. 8A), 10.5 (Fig. 8B) and at 30 °C and pH 11.5 (Fig. 8C – circles). 95% of the equilibrium values were reached within 90 min and the kinetics were not significantly affected within the range of temperatures considered (30 °C and 55 °C). At 55 °C and pH 11.5, the maximum value was reached faster in the sFDG than in the gravimetric case. Whilst around 90 min were required in the gravimetric experiments to get to 95% of the maximum hydration, this time was significantly reduced to 50 min for the sFDG case. As for the analysis shown in Fig. 5, it is likely that the weakest top layers were detached when shear stress was applied from the sFDG, resulting in an underestimation of the swelling time required.

The comparison was extended by transforming sFDG data into mass using Eq. (4). Fig. 9 shows sFDG and gravimetric data represented together and expressed in mass units. In Fig. 9A the absolute mass values from the two experimental techniques are shown, while Fig. 9B represents the difference over time between gravimetric and sFDG data.

Experiments in the milder conditions (30 °C for pH 9.5 and 10.5) showed good agreement as the convergence seen in Fig. 9A was high and the difference showed in Fig. 9B remained flat at values closer to 0.

Experiments at high temperature (55 °C for pH 9.5 and 10.5) showed similar trends for both techniques but the estimated water uptake from sFDG data was systematically higher (1 g) when compared to the measured mass uptake given by gravimetric experiments. Two hypotheses were considered to explain this behaviour:

1. A lift-up effect from sFDG measurements that was favoured at higher temperatures. This would indicate higher elasticity of the soil network with the increase of temperature. As the experimental conditions did not result in any removal of material, the lift-up effect occurred and the thickness values measured were higher. A look at the raw data did not allow assuring this hypothesis. Equilibrium trends were similar to those reported in Fig. 5.
2. Higher amount of water could be lost when removing the excess of water in the gravimetric method. At 55 °C, a lower water viscosity and a consequent higher water mobility could have led to the removal of larger amounts of liquid. The hypothesis was tested and disproved by quantifying the amount of water transferred to the drying paper. The difference in weight between the 'wetted' and 'dried' sample was measured and results showed a loss of approximately 0.2 g and 0.16 g for 55 °C and 30 °C respectively. This effect would only explain 4% of the difference seen between sFDG and gravimetric data.

Differences between sFDG and gravimetric data at high pH (i.e. pH 11.5) became obvious after 20–30 min. The measured mass uptake from the gravimetric tests was higher than the estimated mass uptake from sFDG experiments. If the assumption of molecular incompressibility is still valid, this would indicate a lower

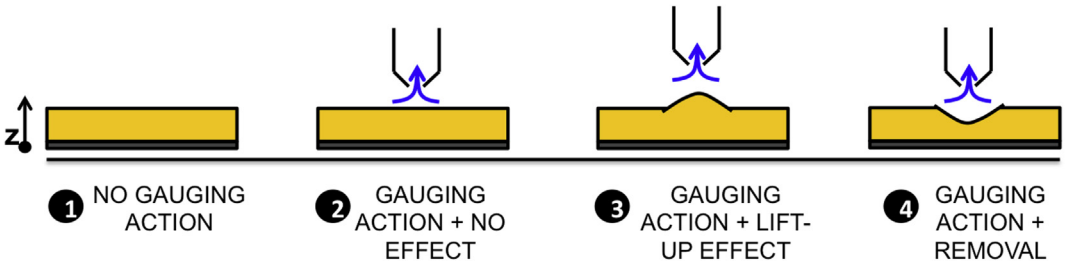

Fig. 6. Schematic of the different scenarios when using the sFDG to measure the thickness of a sample.

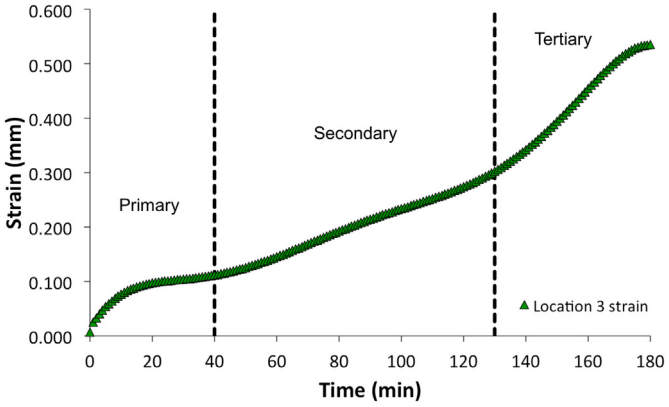

Fig. 7. Strain profile for location 3 in example shown in Fig. 6A.

volume occupied by the solvent molecules within the soil. Two hypothesis were again considered:

1. The presence of electrostatic screening effects between the Na^+ cations in the water and soil network. This would lead to a decrease in the volume of the network. These effects were studied in a similar work by Mercadé-Prieto et al. (2007c) with protein-based systems. Results reported a significant reduction volume as a consequence of the electrostatic effects. However, these interactions occurred at pH higher than 13.3 when only NaOH was added to the solution.
2. The removal of soil layers in those locations with an equilibrium trend (no lift-up and no removal observed). Highly swelled layers could be detached early in the process thus leading to a lower equilibrium thickness value.

4.3. Modelling swelling/hydration

Power law equations (Eq. (1) and Eq. (2)) were applied to the experimental data obtained via gravimetric and sFDG tests. Fig. 10 represents the estimated diffusional exponents, n and n′, as a

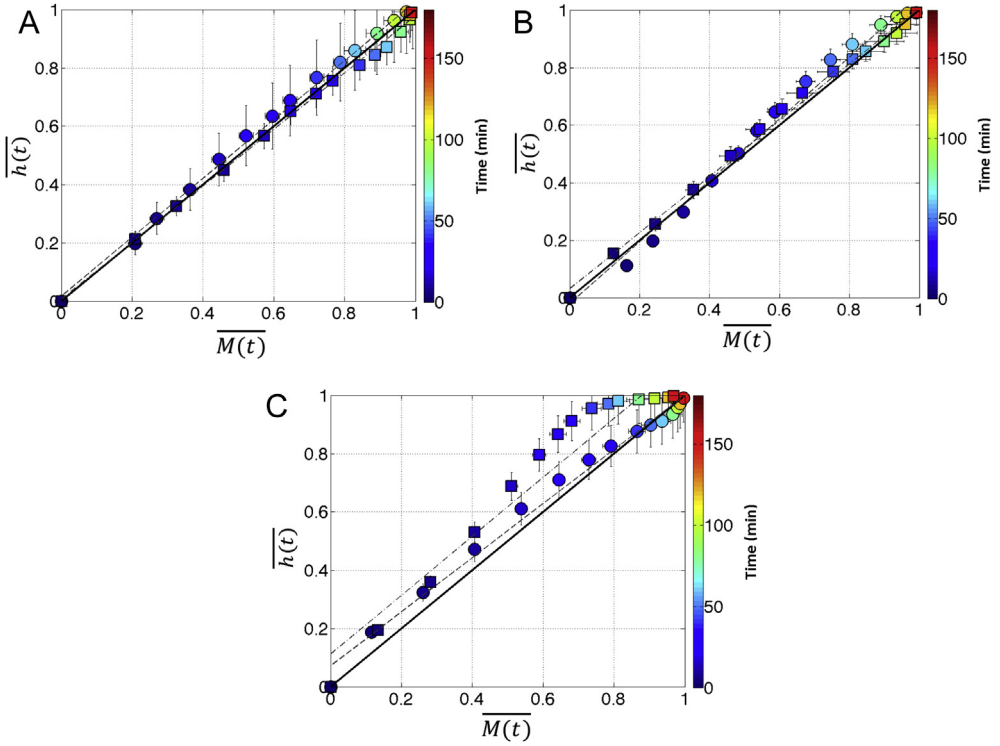

Fig. 8. Normalised height and weight data to compare sFDG and gravimetric tests. A – pH 9.5; B – pH 10.5; C – pH 11.5. Circles – 30 °C; Squares – 55 °C.

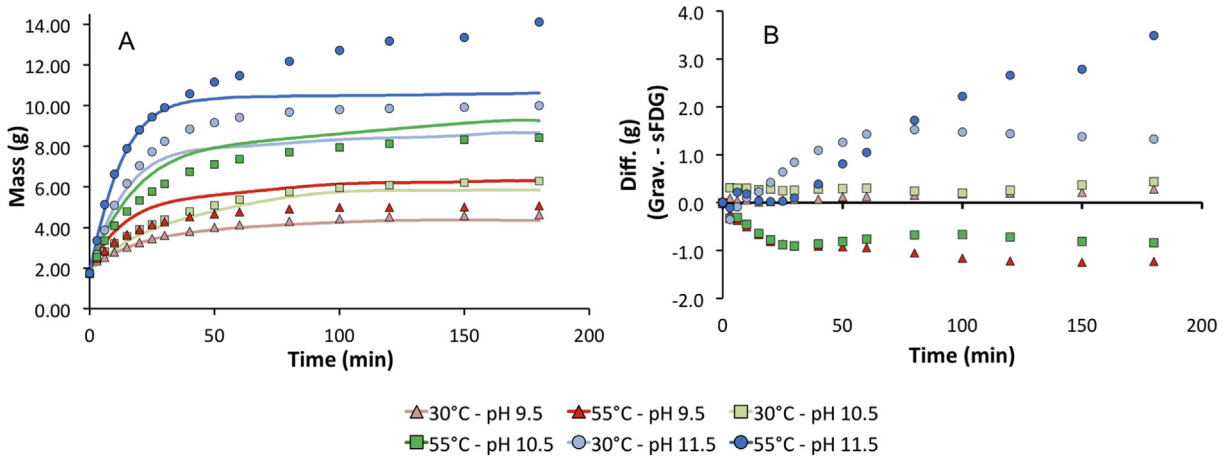

Fig. 9. Comparison of gravimetric and sFDG data in mass units. A – Total mass over time. Lines and dots with same colour represent sFDG and gravimetric data respectively at the same experimental conditions; B – Difference between gravimetric and sFDG data over time. (For interpretation of the references to colour in this figure legend, the reader is referred to the web version of this article.)

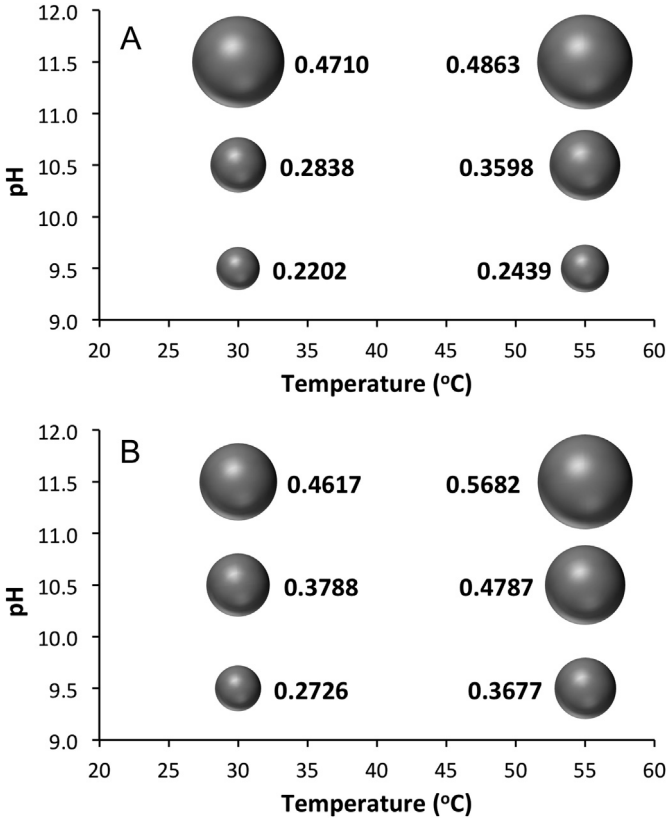

Fig. 10. Diffusional exponent values. A – From gravimetric data (n). B – From sFDG data (n').

function of temperature and pH. The size of the bubbles is related to the value of the exponent.

Results for gravimetric data (Fig. 10A) indicated that pH is the main factor affecting the diffusional exponent (n). Results for sFDG data (Fig. 10B) reported slightly higher values of n′ for the same experimental conditions and a similar effect of pH. The effect of temperature was more pronounced in this case.

Overall, data suggested a Fickian diffusion (Case I) type of transport in all cases ($n < 0.5$). However, as pH increased, there was an increase of 'n' indicating more anomalous or Non-Fickian diffusion (Case II) mechanism. During hydration, as the soil network expanded, the rearrangement became more difficult. Thus, for those cases with higher equilibrium swelling, averaged relaxation times increased and became closer to diffusional times.

Fick's second law (Eq. (3) and Eq. (4)) was used to fit gravimetric data. Fig. 11A illustrates experimental and numerical results for each of the conditions studied. Overall, Fick's second law over-predicted (numerical values above experimental data) results at initial times and under-predicted (numerical values below experimental data) them at longer times. The complexity of the system studied combined with the simplicity of the equation, with only one intrinsic parameters considered (D_F), restricted the quality of the fitting. The incorporation of moving boundaries into the analysis did not provide sufficient flexibility to enhance the results. The initial over prediction can be observed in more detail in Fig. 11B. Fig. 11C represents a linear fit on the data for the first 20 min of the experimental time. The good fit suggests a linear swelling behaviour at this stage. This behaviour was also previously reported for other protein-based gels such as whey protein concentrate (Saikhwan et al., 2010).

Table 3 shows the effective diffusion coefficients (D_F) estimated with Fick's second law together with the slopes of the different linear fits for each case.

Values were in the order of 10^{-11} m^2/s. For the range of pH investigated, the increase from 30 °C to 55 °C showed an increase in the effective diffusion coefficient calculated. This was also observed for increasing pH at the same temperature. Coefficients of determination (R^2) ranged from 0.88 to 0.95.

Non-linear theory (Eq. (5) and Eq. (8)) was used to fit sFDG data. Fig. 12 illustrates experimental and numerical results for each of the conditions studied. The introduction of a higher number of intrinsic parameters increased the goodness of fit to the range of 0.93–0.99.

Table 4 summarises the results estimated by applying the non-linear theory.

Non-linear diffusion coefficients (D_{NL}) were reported at around 10^{-10} m^2/s. The increase from 30 °C to 55 °C showed slightly higher diffusion coefficients at any pH given. The same correlation was observed for increasing pH at a fixed temperature. Flory–Huggins parameter (χ) showed a slight decrease with the increase of temperature and pH. Both, D_{NL} and χ, were likely to change for each experiment as D_{NL} is related to the kinetics of the swelling/diffusion process (temperature dependent) and χ to the interaction between

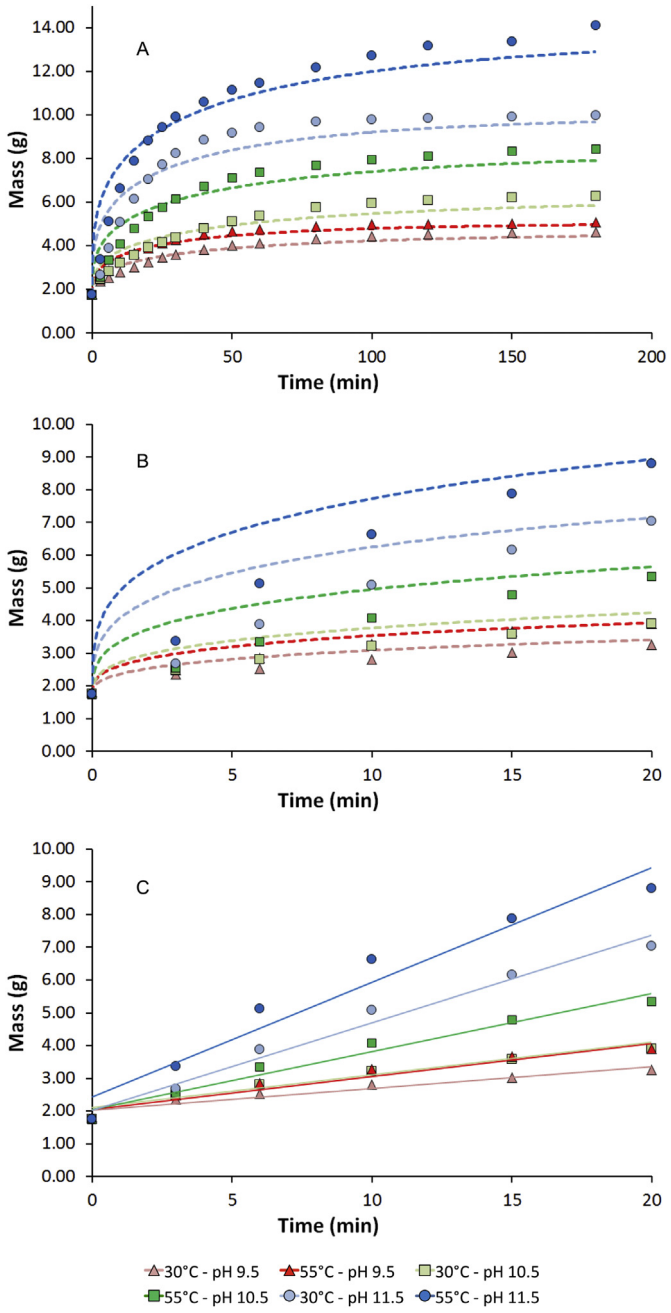

Fig. 11. Comparative results from experimental and numerical data using Fick's second law (dotted lines). A – Data for 180 min; B – Data from the first 20 min; C – Linear fit for data from the first 20 min.

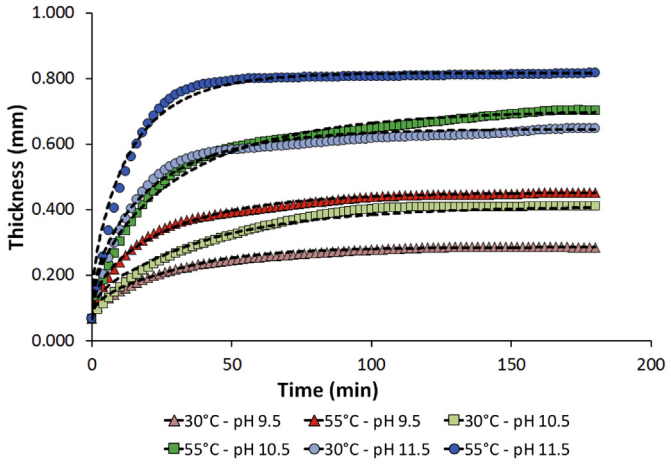

Fig. 12. Comparative results from experimental and numerical data using Non-Linear theory (dotted lines).

Table 3
Fick's second law effective diffusion coefficients and goodness of fit for gravimetric experiments.

Experiment		Fick's law		Linear fit	
Temperature	pH	D_F (m^2/s)	R^2	Slope (g/min)	R^2
30 °C	9.5	$5.5 \cdot 10^{-12}$	0.948	0.07	0.914
55 °C	9.5	$1.0 \cdot 10^{-11}$	0.950	0.10	0.941
30 °C	10.5	$8.6 \cdot 10^{-12}$	0.911	0.10	0.935
55 °C	10.5	$1.9 \cdot 10^{-11}$	0.950	0.18	0.968
30 °C	11.5	$4.1 \cdot 10^{-11}$	0.881	0.27	0.979
55 °C	11.5	$5.4 \cdot 10^{-11}$	0.920	0.35	0.952

the solvent and the polymer (pH dependent). A decrease in the Flory–Huggins parameter indicates a stronger affinity between the solvent and the polymer (Kuhn et al., 2006). Therefore, results showed that the affinity increased with the increase of pH. However, the iteration of χ showed low sensitivity (less accuracy) thus the conclusion made might not be truly reliable. N values estimated remained within a range from $4 \cdot 10^{26}$ to $9.5 \cdot 10^{26}$ m^{-3} with an average value of $5.5 \cdot 10^{26}$ ($\pm 2.1 \cdot 10^{26}$) m^{-3}. The variability seen is caused by the iterative process in the calculations.

Independently of the theory used, diffusion coefficients were lower than the self-diffusion coefficient of water, estimated to be $2.3 \cdot 10^{-9}$ m^2/s (Métais and Mariette, 2003). This suggests an obstruction effect of the soil network on the diffusion of water molecules. The phenomenon was previously reported (Fukuoka et al., 1994). The differences between water self-diffusion coefficient and the ones calculated from these experiments offer an indirect estimation of the resistance offered by the network. The soil network offered the least resistance at high pH and high temperature.

The temperature dependence of the different effective diffusion coefficients estimated was also explored. Eq. (9) was applied to the results shown in Tables 3 and 4. Maximum effective diffusion coefficients (D_0) and activation energies (E_A) were estimated for pairs of data at the same pH and different temperatures. As only two values were used in the calculations, results only represent an indication of the order of magnitude expected. Table 5 summarises the different values obtained.

Activation energies (E_A) estimated showed an average value of 18.4 (±9.0) kJ/mol and 16.4 (±6.7) kJ/mol for Fick's second law and non-linear theory respectively. This compares favourably with what was reported previously in literature (Bello et al., 2010). Maximum effective diffusion coefficient (D_0) showed a wide range of values, being equally (pH 11.5) or higher (pH 9.5 and 10.5) than the one previously reported for the self-diffusion of water.

5. Conclusions

The study showed the importance of temperature and mainly pH as key factors driving the swelling/hydration process on dry egg yolk samples. At high alkalinity (pH 11.5), some of the material was removed when an external surface shear stress was applied. The formation of blisters was also observed in these conditions. The soil network was weaker due to the increase of moisture content and hydrolysis reactions that occurred. The kinetics of the diffusion

Table 4
Non-linear poroelasticity theory results.

Experiment		Non-linear diffusion coefficient D_{NL} (m^2/s)	Flory–Huggings parameter (χ)	Polymer chains per unit volume N (m^{-3})	R^2
T	pH				
30 °C	9.5	$1.5\cdot10^{-10}$	1.00	$9.5\cdot10^{26}$	0.9935
55 °C	9.5	$2.5\cdot10^{-10}$	0.80	$6.0\cdot10^{26}$	0.9910
30 °C	10.5	$3.0\cdot10^{-10}$	0.90	$5.0\cdot10^{26}$	0.9429
55 °C	10.5	$4.0\cdot10^{-10}$	0.80	$4.0\cdot10^{26}$	0.9828
30 °C	11.5	$4.5\cdot10^{-10}$	0.65	$4.5\cdot10^{26}$	0.9697
55 °C	11.5	$9.0\cdot10^{-10}$	0.00	$4.0\cdot10^{26}$	0.9355

Table 5
Activation energies and maximum effective diffusion coefficients estimated.

Theory	T	pH	Diffusion coefficient (m^2/s)	E_A (kJ/mol)	D_0 (m^2/s)
Fick's second law	30 °C	9.5	$5.5\cdot10^{-12}$	19.8	$1.40\cdot10^{-8}$
	55 °C	9.5	$1.0\cdot10^{-11}$		
	30 °C	10.5	$8.6\cdot10^{-12}$	26.2	$2.83\cdot10^{-7}$
	55 °C	10.5	$1.9\cdot10^{-11}$		
	30 °C	11.5	$4.1\cdot10^{-11}$	9.1	$1.52\cdot10^{-9}$
	55 °C	11.5	$5.4\cdot10^{-11}$		
	Mean			18.4 (±9.0)	$9.9\cdot10^{-8}$ ($\pm1.6\cdot10^{-7}$)
Non-linear poroelasticity theory	30 °C	9.5	$1.5\cdot10^{-10}$	16.9	$1.2\cdot10^{-7}$
	55 °C	9.5	$2.5\cdot10^{-10}$		
	30 °C	10.5	$3.0\cdot10^{-10}$	9.5	$1.3\cdot10^{-8}$
	55 °C	10.5	$4.0\cdot10^{-10}$		
	30 °C	11.5	$4.5\cdot10^{-10}$	22.9	$4.0\cdot10^{-6}$
	55 °C	11.5	$9.0\cdot10^{-10}$		
	Mean			16.4 (±6.7)	$1.4\cdot10^{-6}$ ($\pm2.3\cdot10^{-6}$)

process did not show significant differences within the range of conditions studied. 95% of the maximum swelling was reached approximately after 90 min.

The use of the power-law model suggested a Fickian diffusion transport model. The adaptation of the equation to fit sFDG data produced comparable results. The increase of temperature and pH led the mass transfer process towards an anomalous scenario. The sample network needed to accommodate higher volumes of liquid over the same time period as the maximum swelling was reached at the same time. Therefore, the network rearrangement became more difficult.

Two theoretical approaches were used to estimate effective diffusion coefficients. Fick's second law (with moving boundaries) showed lower accuracy in predictions than the non-linear theory. The estimation of activation energies in the analysis of the temperature dependence of the diffusion coefficient was also possible.

Acknowledgements

This research was funded by the Engineering and Physical Science Research Council (EPSRC) (Grant number: EP/G036713/1) and industrially sponsored by Procter & Gamble. The authors would like to thank Zayeed Alam and Carlos Amador for their help and useful discussion.

References

Alfrey, T., Gurnee, E.F., Lloyd, W.G., 1966. Diffusion in glassy polymers. J. Polym. Sci. Part C 12, 249–261. http://dx.doi.org/10.1002/polc.5070120119.
Bakalis, S., Kyritsi, A., Karathanos, V.T., Yanniotis, S., 2009. Modeling of rice hydration using finite elements. J. Food Eng. 94, 321–325. http://dx.doi.org/10.1016/j.jfoodeng.2009.03.023.
Bello, M., Tolaba, M.P., Aguerre, R.J., Suarez, C., 2010. Modeling water uptake in a cereal grain during soaking. J. Food Eng. 97, 95–100. http://dx.doi.org/10.1016/j.jfoodeng.2009.09.020.
Biot, M.A., 1941. General theory of three dimensional consolidation. J. Appl. Phys. 12, 155–164.
Bird, M.R., Fryer, P.J., 1991. An experimental study of the cleaning of surfaces fouled by whey proteins. Food Bioprod. Process. Trans. Inst. Chem. Eng. Part C 69, 13–21.
Bird, R.B., Stewart, W.E., Lightfoot, E.N., 2007. Transport Phenomena, Chemistry &…. John Wiley & Sons.
Booth, D.T., 2003. Composition and energy density of eggs from two species of freshwater turtle with twofold ranges in egg size. Comp. Biochem. Physiol. A. Mol. Integr. Physiol. 134, 129–137. http://dx.doi.org/10.1016/S1095-6433(02)00216-7.
Briffaz, A., Bohuon, P., Méot, J.M., Dornier, M., Mestres, C., 2014. Modelling of water transport and swelling associated with starch gelatinization during rice cooking. J. Food Eng. 121, 143–151. http://dx.doi.org/10.1016/j.jfoodeng.2013.06.013.
Chapwanya, M., Misra, N.N., 2015. A soft condensed matter approach towards mathematical modelling of mass transport and swelling in food grains. J. Food Eng. 145, 37–44. http://dx.doi.org/10.1016/j.jfoodeng.2014.08.010.
Chen, G., Campanella, O.H., Purkayastha, S., 2007. A dynamic model of crosslinked corn starch granules swelling during thermal processing. J. Food Eng. 81, 500–507. http://dx.doi.org/10.1016/j.jfoodeng.2006.12.001.
Davey, M.J., Landman, K.A., McGuinness, M.J., Jin, H.N., 2002. Mathematical modeling of rice cooking and dissolution in beer production. AIChE J. 48, 1811–1826. http://dx.doi.org/10.1002/aic.690480821.
Denmat, M., Anton, M., Gandemer, G., 1999. Protein denaturation and emulsifying properties of plasma and granules of egg yolk as related to heat treatment. J. Food Sci. 64, 194–197. http://dx.doi.org/10.1111/j.1365-2621.1999.tb15863.x.
DuPont, 2012. US Consumer Dishwashing Study [WWW Document]. URL. http://fhc.biosciences.dupont.com/consumer-trends/consumer-studies/us-consumer-dishwashing-study/ (accessed 12.5.14).
Flory, P.J., Rehner Jr., J., 1943. Statistical mechanics of cross-linked polymer networks II. swelling. J. Chem. Phys. 11, 521–526.
Fryer, P.J., Christian, G.K., Liu, W., 2006. How hygiene happens: physics and chemistry of cleaning. Soc. Dairy Technol. 59, 76–84. http://dx.doi.org/10.1111/j.1471-0307.2006.00249.x.
Fukuoka, M., Watanabe, H., Mihori, T., Shimada, S., 1994. Moisture diffusion in a dry soybean seed measured using pulsed-field-gradient NMR. J. Food Eng. 23, 533–541. http://dx.doi.org/10.1016/0260-8774(94)90110-4.
Ganji, F., 2010. Theoretical description of hydrogel swelling: a review. Iran. Polym. 19, 375–398.
Gibbs, J.W., 1906. The Scientific Papers of Willian Gibbs [WWW Document]. URL. http://books.google.com/books?id=-neYVEbAm4oC&oe=UTF-8 (accessed 12.9.13).
Gordon, P.W., 2012. Development of a Scanning Fluid Dynamic Gauge for Cleaning Studies. Thesis. University of Cambridge.
Gordon, P.W., Brooker, A.D.M., Chew, Y.M.J., Letzelter, N., York, D.W., Wilson, D.I., 2012. Elucidating enzyme-based cleaning of protein soils (gelatine and egg yolk) using a scanning fluid dynamic gauge. Chem. Eng. Res. Des. 90, 162–171. http://dx.doi.org/10.1016/j.cherd.2011.07.007.

Gordon, P.W., Brooker, A.D.M., Chew, Y.M.J., Wilson, D.I., York, D.W., 2010. A scanning fluid dynamic gauging technique for probing surface layers. Meas. Sci. Technol. 21, 085103. http://dx.doi.org/10.1088/0957-0233/21/8/085103.

Hong, W., Zhao, X., Zhou, J., Suo, Z., 2008. A theory of coupled diffusion and large deformation in polymeric gels. J. Mech. Phys. Solids 56, 1779–1793. http://dx.doi.org/10.1016/j.jmps.2007.11.010.

Kruif, C.G.K., De Anema, S.G., Zhu, C., Havea, P., Coker, C., 2015. Food hydrocolloids water holding capacity and swelling of casein hydrogels. Food Hydrocoll. 44, 372–379. http://dx.doi.org/10.1016/j.foodhyd.2014.10.007.

Kuhn, C.R., Soares, G.J.D., Kuhn, P.S., 2006. Electrostatic contribution to polymer gels. Colloids surfaces A physicochem. Eng. Asp. 281, 184–189. http://dx.doi.org/10.1016/j.colsurfa.2006.02.037.

Labuza, T., Hyman, C., 1998. Moisture migration and control in multi-domain foods. Trends Food Sci. Technol. 9, 47–55. http://dx.doi.org/10.1016/S0924-2244(98)00005-3.

Malumba, P., Jacquet, N., Delimme, G., Lefebvre, F., Béra, F., 2013. The swelling behaviour of wheat starch granules during isothermal and non-isothermal treatments. J. Food Eng 114, 199–206. http://dx.doi.org/10.1016/j.jfoodeng.2012.08.010.

McKeen, L.W., 2015. Introduction to creep, polymers, plastics and elastomers. In: The Effect of Creep and Other Time Related Factors on Plastics and Elastomers. Elsevier Inc. http://dx.doi.org/10.1016/B978-0-323-35313-7.00001-8.

Mehrer, H., 2007. Diffusion in Solids: Fundamentals, Methods, Materials, Diffusion-controlled Processes, Springer Series in Solid-state Sciences. Springer.

Mercadé-Prieto, R., Chen, X.D., 2006. Dissolution of whey protein concentrate gels in alkali. AIChE J. 52, 792–803. http://dx.doi.org/10.1002/aic.10639.

Mercadé-Prieto, R., Falconer, R.J., Paterson, W.R., Wilson, D.I., 2007a. Swelling and dissolution of beta-lactoglobulin gels in alkali. Biomacromolecules 8, 469–476. http://dx.doi.org/10.1021/bm060553n.

Mercadé-Prieto, R., Paterson, W.R., Wilson, D.I., 2007b. The pH threshold in the dissolution of beta-lactoglobulin gels and aggregates in alkali. Biomacromolecules 8, 1162–1170. http://dx.doi.org/10.1021/bm061100l.

Mercadé-Prieto, R., Paterson, W.R., Wilson, D.I., 2009. Effect of salts on the alkaline degradation of β-lactoglobulin gels and aggregates: existence of a dissolution threshold. Food Hydrocoll. 23, 1587–1595. http://dx.doi.org/10.1016/j.foodhyd.2008.11.007.

Mercadé-Prieto, R., Sahoo, P.K., Falconer, R.J., Paterson, W.R., Ian Wilson, D., 2007c. Polyelectrolyte screening effects on the dissolution of whey protein gels at high pH conditions. Food Hydrocoll. 21, 1275–1284. http://dx.doi.org/10.1016/j.foodhyd.2006.09.015.

Métais, A., Mariette, F., 2003. Determination of water self-diffusion coefficient in complex food products by low field 1H PFG-NMR: comparison between the standard spin-echo sequence and the T1-weighted spin-echo sequence. J. Magn. Reson. 165, 265–275. http://dx.doi.org/10.1016/j.jmr.2003.09.001.

Mezzenga, R., Schurtenberger, P., Burbidge, A., Michel, M., 2005. Understanding foods as soft materials. Nat. Mater 4, 729–740. http://dx.doi.org/10.1038/nmat1496.

Mine, Y., Zhang, H., 2013. Biochemistry of foods. In: Biochemistry of Foods, third ed. Elsevier. http://dx.doi.org/10.1016/B978-0-08-091809-9.00005-4.

Mitchell, S.L., O'Brien, S.B.G., 2012. Asymptotic, numerical and approximate techniques for a free boundary problem arising in the diffusion of glassy polymers. In: Applied Mathematics and Computation, pp. 376–388. http://dx.doi.org/10.1016/j.amc.2012.06.026.

Oztop, M.H., McCarthy, K.L., 2011. Mathematical modeling of swelling in high moisture whey protein gels. J. Food Eng 106, 53–59. http://dx.doi.org/10.1016/j.jfoodeng.2011.04.007.

Peppas, N.A., Brannon-Peppas, L., 1994. Water diffusion and sorption in amorphous macromolecular systems and foods. J. Food Eng 22, 189–210. http://dx.doi.org/10.1016/0260-8774(94)90030-2.

Peppas, N.A., Sinclair, J.L., 1983. Anomalous transport of penetrants in glassy polymers. Colloid Polym. Sci. 261, 404–409.

Saikhwan, P., Mercadé-Prieto, R., Chew, Y.M.J., Gunasekaran, S., Paterson, W.R., Wilson, D.I., 2010. Swelling and dissolution in cleaning of whey protein gels. Food Bioprod. Process 88, 375–383. http://dx.doi.org/10.1016/j.fbp.2010.09.006.

Sam Saguy, I., Marabi, A., Wallach, R., 2005. New approach to model rehydration of dry food particulates utilizing principles of liquid transport in porous media. Trends Food Sci. Technol. 16, 495–506. http://dx.doi.org/10.1016/j.tifs.2005.07.006.

Thomas, N., Windle, A., 1982. A theory of case II diffusion. Polym. Guildf. 23, 529–542.

Thomas, N.L., Windle, A.H., 1980. A deformation model for case II diffusion. Polym. Guildf. 21, 613–619.

Tsutsui, T., 1988. Functional properties of heat-treated egg yolk low density lipoprotein. J. Food Sci. 53, 1103–1106.

Tuladhar, T., Paterson, W.R., Macleod, N., Wilson, D.I., 2000. Development of a novel non-contact proximity gauge for thickness measurement of soft deposits and its application in fouling studies. Can. J. Chem. Eng. 78, 935–947. http://dx.doi.org/10.1002/cjce.5450780511.

Tuladhar, T.R., Paterson, W.R., Wilson, D.I., 2002. Thermal conductivity of whey protein films undergoing swelling. Food Bioprod. Process 80, 332–339. http://dx.doi.org/10.1205/096030802321154862.

Van Der Sman, R.G.M., 2012. Soft matter approaches to food structuring. Adv. Colloid Interface Sci. 176–177, 18–30. http://dx.doi.org/10.1016/j.cis.2012.04.002.

Van Der Sman, R.G.M., 2014. Moisture transport in swelling media modelled with a lattice Boltzmann scheme having a deforming lattice. J. Food Eng 124, 54–63. http://dx.doi.org/10.1016/j.jfoodeng.2013.09.033.

Van der Sman, R.G.M., van der Goot, A.J., 2009. The science of food structuring. Soft Matter 5, 501–510. http://dx.doi.org/10.1039/b718952b.